Contrib Mineral Petrol (2006) 152: 43–51
DOI 10.1007/s00410-006-0093-4

ORIGINAL PAPER

Philip Skemer · Ikuo Katayama · Shun-ichiro Karato

Deformation fabrics of the Cima di Gagnone peridotite massif, Central Alps, Switzerland: evidence of deformation at low temperatures in the presence of water

Received: 30 August 2005 / Accepted: 6 March 2006 / Published online: 27 April 2006

Abstract We report a new observation of the olivine B-type lattice-preferred orientation (LPO), from the garnet peridotite at Cima di Gagnone, Switzerland. The olivine B-type fabric forms at low temperatures and/or high stress in the presence of water, and is of particular interest because it may be used to explain the trench-parallel shear-wave splitting that is often observed at subduction zones. In conjunction with the olivine B-type fabric, we have found strong orthopyroxene LPO that is identical to those formed under water-free conditions. This suggests that water may not have a significant effect on orthopyroxene fabric. From the olivine microstructure, we determine that a stress of 22 ± 8 MPa was applied during the deformation event that formed the olivine LPO. Using an olivine flow-law, and assuming geological strain-rates, we determine the temperature of deformation to be 800 ± 175°C. This does not preclude an ultra-deep origin for the ultramafic rocks at Cima di Gagnone, but indicates that much of the deformation recorded in the microstructure occurred at modest temperatures.

Introduction

When the upper mantle deforms, olivine develops a lattice-preferred orientation (LPO) that is detectable as seismic anisotropy. Recent experimental work by Jung and Karato (2001a) and Katayama et al. (2004) has shown that in the presence of water olivine can adopt several distinct LPOs, which alter the typical relationship between deformation and seismic anisotropy (Nicolas and Christensen 1987; Ben Ismail and Mainprice 1998). Of particular interest amongst these is the "B-type" fabric, which forms by deformation that is predominantly accommodated by the [001](010) slip system. This type of deformation generates a shear-wave splitting signature with the polarization of the fast shear-wave normal to the direction of flow, within the shear-plane (Katayama and Karato 2006; Kneller et al. 2005). Thus, the B-type fabric can explain the trench-parallel shear-wave splitting often observed in arc environments (e.g. Russo and Silver 1994), without invoking trench-parallel flow induced by local plate motions (Fischer et al. 1998; Smith et al. 2001; Mehl et al. 2003), oblique subduction (Hall et al. 2000), slab roll-back (Peyton et al. 2001), or strain partitioning in partially molten peridotite (Holtzman et al. 2003).

Because experimental rock deformation studies are necessarily conducted at much higher strain-rates (typically 10^{-4} to 10^{-6} s^{-1}) than those in Earth (10^{-13} to 10^{-15} s^{-1}), it is not straightforward to apply laboratory data to Earth's interior. In the initial study of olivine fabrics by Jung and Karato (2001a), the B-type fabric was found only at high stress (> 340 MPa), at temperatures of ~1,200°C. However, recent experimental work by Katayama and Karato (2006) has found that at lower temperatures the boundary between the B-type and C-type fabrics occurs at lower stresses. To further bridge the gap between experiments and nature it is helpful to identify these experimentally produced fabrics in naturally deformed rocks, and constrain the temperature, pressure, and chemical environment in which the deformation occurred. In this study, we report the identification of B-type fabrics in the garnet-bearing peridotite massif at Cima di Gagnone, Switzerland, and use microstructural information to constrain the conditions of deformation. B-type fabrics have previously been found in the Yushigou peridotite, China (Song and Su 1998), in the Sambagawa metamorphic belt, S.W. Japan (Yoshino 1961; Mizukami et al. 2004), and in the Almklovdalen massif, S. Norway (Cordellier et al. 1981). However, of these studies, only Mizukami et al.

Communicated by T.L. Grove

P. Skemer (✉) · I. Katayama · S. Karato
Department of Geology and Geophysics, Yale University,
PO Box 208109, New Haven, CT 06520-8109, USA
E-mail: philip.skemer@yale.edu
Tel.: +1-203-4325791
Fax: +1-203-4323134

(2004) were able to determine the conditions of deformation during the development of the LPO.

There is one previous report on olivine LPO from the Cima di Gagnone massif, in which Frese et al. (2003) document the presence of the C-type fabric, which is characterized by deformation on the [001](100) slip system. In a more comprehensive description of the locality, Frese (2001) also shows LPO data from one sample that appears to be an example of a B-type fabric. C-type fabrics have also been extensively described at nearby Alpe Arami, an ultramafic body that lies in the same horizon of the Adula/Cima Lunga nappe (Mockel 1969; Buiskool Toxopeus 1976; Frese 2001).

Although several olivine fabrics have been documented in experiments and in natural rocks, there have been limited comparable studies of orthopyroxene fabrics. In naturally deformed rocks, orthopyroxene is generally found to exhibit only one type of LPO, resulting from deformation on the [001](100) slip system (Christensen and Lundquist 1982). In this study, we have also examined the orthopyroxene LPO to compare the LPOs of olivine and orthopyroxene deformed under similar conditions.

Alpe Arami, and to a certain extent Cima di Gagnone, have been the subject of an ongoing controversy over their depth of origin. Some groups have advocated ultra-deep (>300 km) origins (e.g. Dobrzhinetskaya et al. 1996; Green et al. 1997; Bozhilov et al. 1999), while others have argued for shallower origins (e.g. Hacker et al. 1997; Nimis and Trommsdorff 2001). While we do not propose to resolve this controversy here, we have used our microstructural analyses of Cima di Gagnone and others' analyses of Alpe Arami to place new constraints on the conditions of deformation. These results do not constrain the maximum depth of origin of these rocks, but may provide new insight into their metamorphic and deformational history.

Geologic setting

Cima di Gagnone, Alpe Arami, and numerous smaller ultramafic bodies appear along a narrow tectonostratigraphic horizon in the upper part of the Adula/Cima Lunga nappe, in the Central Alps, Ticino, Switzerland (Pfiffner and Trommsdorff 1998) (Fig. 1). The Adula/Cima Lunga nappe is thought to have been part of the former European continental margin (Schmid et al. 1990), which was subducted beneath the Adriatic Plate during the Alpine orogeny, and subsequently exhumed. There are a number of small ultramafic bodies that outcrop at Cima di Gagnone, although garnet-bearing peridotite has only been found at the core of one large (~50 m) lens (outcrop Mg160; Evans and Trommsdorff 1978). The garnet-bearing core is small (~4 m) and lherzolitic in composition. Frese et al. (2003) report modal abundances of 65% olivine, 15% clinopyroxene, 10% orthopyroxene, and 10% garnet. Surrounding the core is a mantle of peridotite that has been retrogressed at amphibolite conditions and contains various amounts of chlorite, amphibole, and spinel, replacing garnet and clinopyroxene. Although the lens is petrologically varied, the structure is fairly constant throughout (Evans and Trommsdorff 1978).

Methods

Several samples were collected from both the garnet-bearing and the retrogressed portions of the Cima di Gagnone peridotite. Thin-sections were cut parallel to the lineation and perpendicular to the foliation for microstructural analysis. The LPO of olivine, orthopyroxene, and clinopyroxene (when present) was measured for each sample using the electron backscatter diffraction (EBSD) technique (Prior et al. 1999). EBSD measurements were made on an FEI XL-30 ESEM-FEG, with an accelerating voltage of 20 kV and a beam current of 2.4 nA at a working distance of 20 mm. The sample was scanned in a grid pattern with a step size roughly equal to the mean grain-size. At each point, the EBSD pattern was indexed manually to guarantee an accurate solution and to ensure that individual grains were not counted multiple times. For olivine, a minimum of 150 discrete grains were measured for each sample (Skemer et al. 2005). Seismic anisotropy was calculated from the orientation data (Mainprice 1990) using elastic constants at 3 GPa and 800°C for olivine (Isaak 1992; Abramson et al. 1997), orthopyroxene (Frisillo and Barsch 1972; Chai et al. 1997), and clinopyroxene (Collins and Brown 1998). Dislocations in olivine were observed by the oxidation decoration technique (Kohlstedt et al. 1976) using both an optical microscope and a scanning electron microscope (Karato 1987).

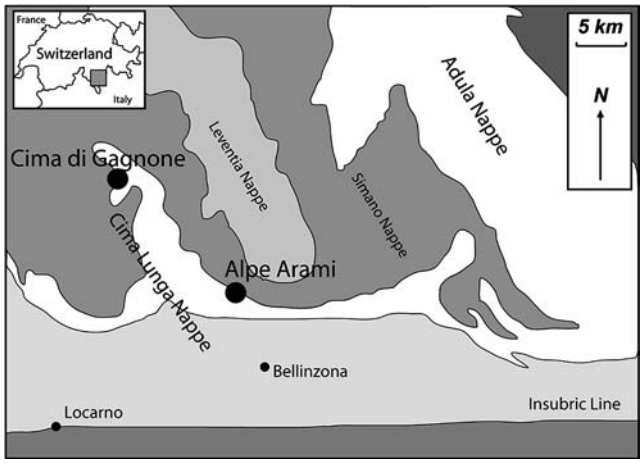

Fig. 1 Geologic map of the region showing the basic nappe structure and the locations of Cima di Gagnone and Alpe Arami. Modified from Evans and Trommsdorff (1978)

Results

Microstructural observations

All samples exhibit a well-developed foliation and lineation, defined by the shape-preferred orientation of the olivine, pyroxenes, and garnet when present. Typical microstructures for the garnet-bearing and retrogressed peridotites are shown in Fig. 2a, b, respectively. Olivine grains are elongated, with a mean grain-size of ~1 mm, as determined by the mean-intercept technique, using a stereographic correction of factor of 1.5. In thin-section, olivine shows no evidence of internal deformation. Often, several grains of similar orientations are found in elongate clusters, suggesting that these grains were derived from a single grain by dynamic recrystallization. Applying the grain-size piezometer of Jung and Karato (2001b), we determine that the stress during this deformation event was 22 ± 8 MPa. The uncertainty in the stress estimate comes from the error in the laboratory measurement of grain-size. Olivine grains contain abundant inclusions of ilmenite, which are oriented parallel to the olivine [010] axis. These inclusions are heterogeneously distributed, but are found in virtually all grains. Dislocations are often seen associated with the ilmenite inclusions. This is illustrated in Fig. 2c where dislocations are shown extending from the tips of ilmenite inclusions. Although there are few subgrain boundaries, arrays of straight, parallel dislocations can occasionally be seen in decorated samples. The orientations of these tilt-walls and their constituent dislocation lines, determined by EBSD and optical microscopy, indicate that the deformation that formed the dislocation microstructure primarily involved the [100](010) and [100](001) slip systems. The density of these dislocations is related to the stress of this deformation event. Applying an olivine dislocation density piezometer, we determine that the stress during this deformation event was 28 ± 6 MPa (Karato and Jung 2003). Orthopyroxene grains are roughly the same size as the olivine grains and are often concentrated in long, narrow bands that parallel the foliation. Some bands can be a centimeter in length, and contain several individual grains aligned in series. Orthopyroxene grains display a well-developed subgrain microstructure (Fig. 2a, b). In the garnet-bearing peridotite, the garnet is highly deformed and concentrated in millimeter scale bands, with numerous pyroxene and amphibole inclusions. There is no evidence, however, of pyroxene exsolution from a majoritic precursor. In the retrogressed peridotites, chlorite and amphibole appear in millimeter scale clusters with no shape-preferred orientation (Fig. 2c).

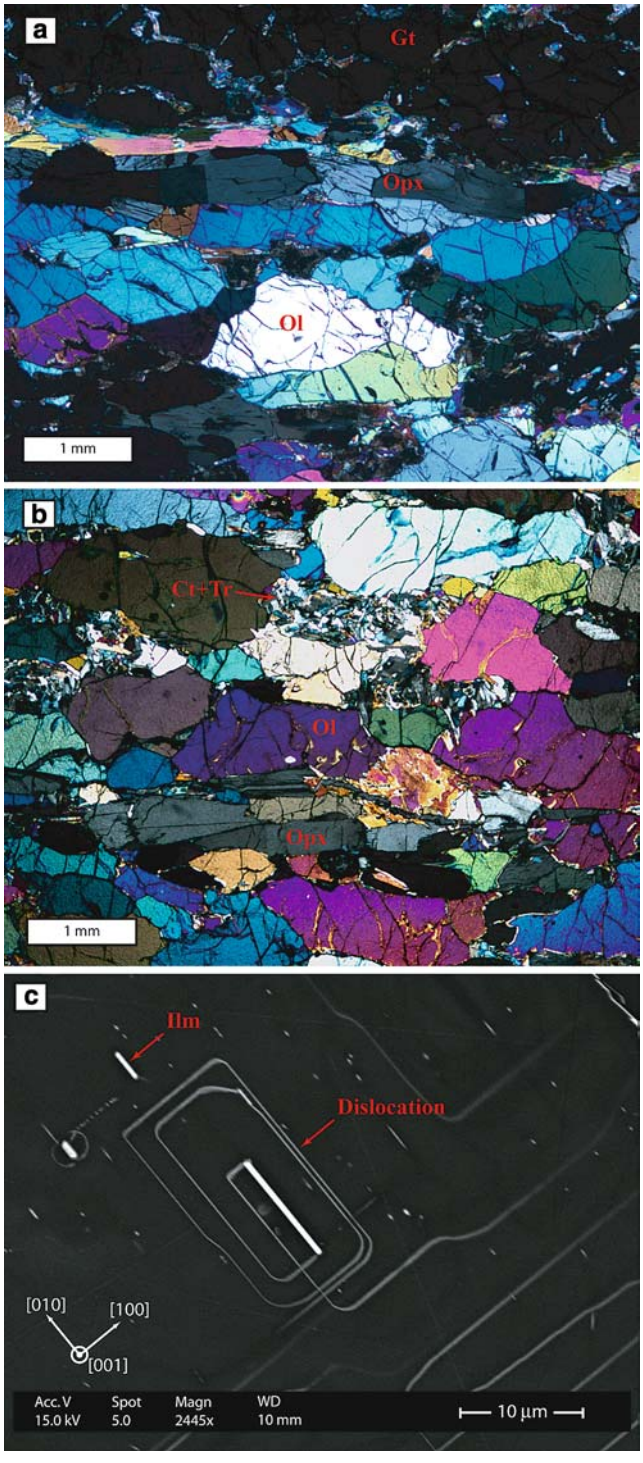

Fig. 2 **a** Photomicrograph of a garnet lherzolite (sample PK-02) and **b** a retrogressed peridotite (sample PK-06) from Cima di Gagnone. *Ol* olivine, *Opx* orthopyroxene, *Gt* garnet, *Ct* chlorite, *Tr* tremolite. The photomicrographs are oriented so that the lineation is East–West, and the pole to the foliation is North–South. Most minerals are elongated parallel to the shear-direction, particularly the orthopyroxene and the garnet. Orthopyroxene has a well-developed subgrain microstructure. Chlorite + tremolite clusters in the retrogressed peridotite show little to no shape-preferred orientation. **c** Backscatter image of a decorated olivine grain from sample PK-02. *Ilm* ilmentite. Dislocations can be seen nucleating from the ilmenite rods, suggesting that the dislocation microstructure post-dates the precipitation of the ilmenite

Lattice-preferred orientation

The olivine, orthopyroxene, and clinopyroxene LPOs are shown in Fig. 3. The pole figures are oriented so

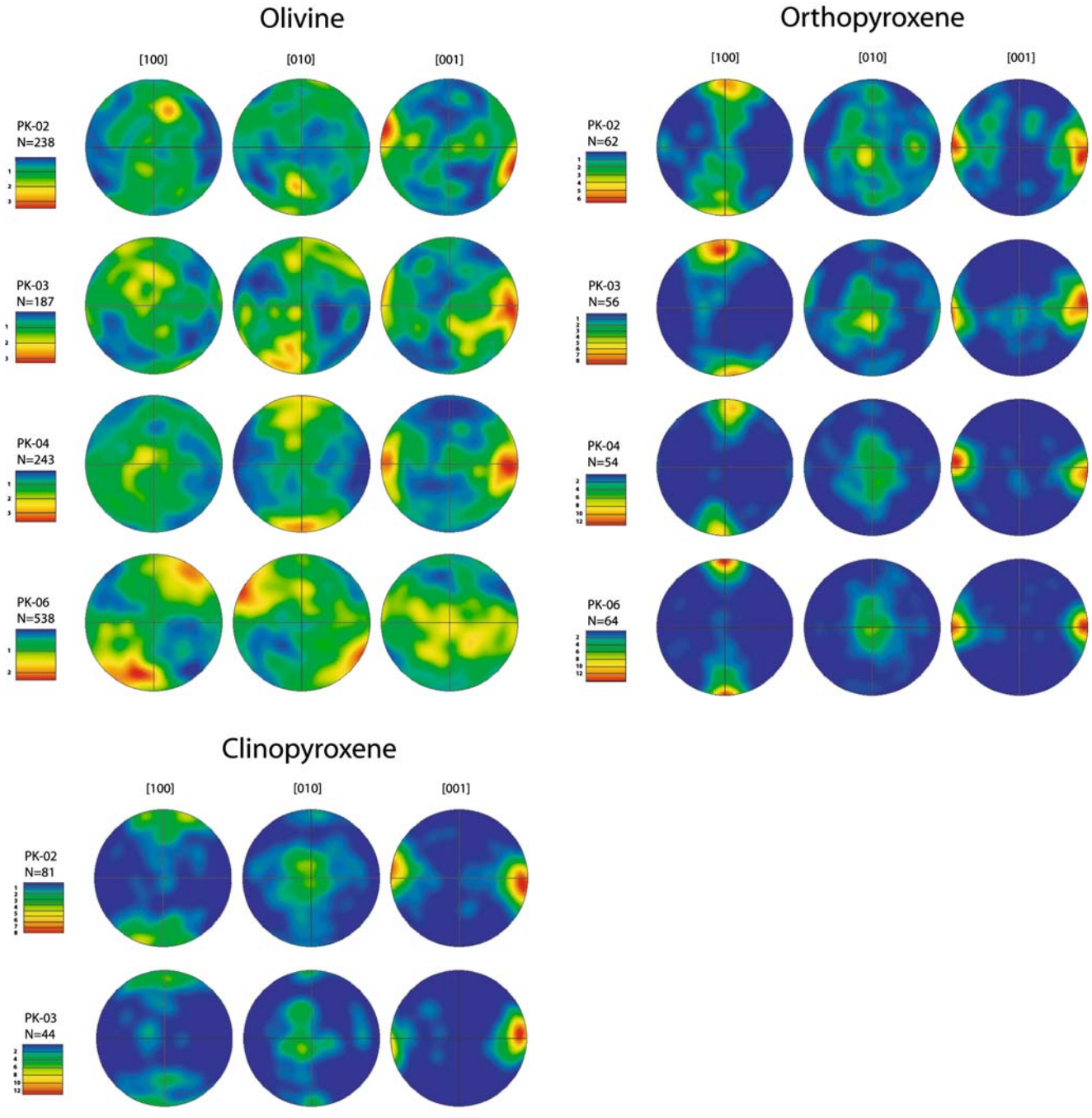

Fig. 3 Pole figures showing the olivine, orthopyroxene, and clinopyroxene lattice-preferred orientation. *N* is the number of discrete grains measured. The pole figures (equal area, *upper-hemispheric projections*) are oriented so that the lineation is E–W and the pole to the foliation is N–S. Samples PK-02, PK-03, and PK-04 show olivine B-type fabrics. Sample PK-06 shows an anomalous fabric that would seem to be characterized by deformation in the b = [010] direction. All samples show a strong orthopyroxene fabric of typical orientation. Samples PK-02 and PK-03 also show a strong clinopyroxene fabric with [001] axes parallel to the lineation and [100] axes normal to the foliation. Samples PK-04 and PK-06 have no clinopyroxene, so no pole figures are shown

that the lineation is E–W and the pole to the foliation is N–S. Samples PK-02, PK-03 (garnet lherzolites), and PK-04 (a retrogressed peridotite), display reasonably clear olivine B-type fabrics, with [001] axes parallel to the lineation and [010] axes normal to the foliation. Sample PK-06, another retrogressed peridotite, has an anomalous fabric with the [010] axes closest to the lineation, and the [100] axes closest to the foliation normal. Because the [010] axes are clustered close the lineation direction, deformation would seem to be characterized by a [010] Burgers vector. This type of fabric has not, to our knowledge, been observed elsewhere, although TEM studies have identified [010] Burgers vectors in other naturally deformed olivine

samples (Fujino et al. 1993). The orthopyroxene in all samples shows a very strong preferred orientation, with [001] axes parallel to the lineation and [100] axes normal to the foliation. This LPO is typical of mantle-deformed orthopyroxene, although the fabric is unusually strong (Christensen and Lundquist 1982; Nicolas and Christensen 1987). The clinopyroxene LPO is also strong, and like orthopyroxene is characterized by [001] axes parallel to the lineation and [100] axes normal to the foliation.

Seismic anisotropy

Figure 4 shows the calculated seismic anisotropy for the garnet peridotite sample PK-02. The pole figures are oriented parallel to the shear-plane with the lineation oriented E–W to facilitate comparisons with seismic data. The seismic anisotropy generated by olivine, orthopyroxene, and clinopyroxene are shown separately, and are also shown combined in normalized modal proportions (olivine 72%; clinopyroxene 17%; orthopyroxene 11%; Frese et al. 2003). Garnet was not considered because it is elastically isotropic and represents only a small volume fraction of the samples.

In sample PK-02, as in all B-type fabrics, the seismically fast olivine *a*-axes are clustered normal to the lineation, in the shear-plane. Thus, P-waves propagate fastest in this direction. In both orthopyroxene and clinopyroxene, the *a*-axes are clustered normal to the shear-plane, with the intermediate *c*-axis parallel to the shear-direction. Thus, P-waves in orthopyroxene and clinopyroxene propagate fastest normal to the shear-plane. P-wave azimuthal anisotropy is moderate in olivine and orthopyroxene at 2.6 and 2.9%, respectively. P-wave azimuthal anisotropy is relatively large in clinopyroxene (8.1%), which reflects the strength of the clinopyroxene fabric, as well as its strong single crystal anisotropy. Combined with olivine in modal proportions, the pyroxenes have a significant influence on the P-wave anisotropy. In the aggregate, the fastest propagation direction for P-waves is normal to the shear-plane, and the slowest direction is parallel to the shear-direction.

In olivine and clinopyroxene, the polarization direction of the faster shear-wave passing through the shear-plane is normal to the direction of flow. In orthopyroxene the faster shear-wave is polarized parallel to the direction of flow. When combined in aggregate, the polarization of the fast shear-wave passing through the shear-plane is normal to the direction of flow.

Discussion

Deformation history

The microstructural observations reported above provide some primary constraints on the relative timing of deformation events. In olivine, the dislocation microstructure we observe is consistent with deformation on the [100](010) and [100](001) slip systems. We do not see any evidence of [001](010) slip, as would be expected if the dislocation microstructure was formed during the deformation event that formed the B-type LPO. From laboratory experiments it is known that a dislocation microstructure can be altered with as little as a 1% strain (Durham et al. 1977). However, to alter LPO requires several tens of percent strain (Zhang and Karato 1995). Thus, the deformation event that produced the dislocation microstructure must have occurred after the deformation that produced the LPO and must have accommodated minimal strain so as not to alter the preexisting LPO. If this late stage deformation event was extremely short, it is possible that some [001](010) dislocations would still be present in the sample, however none were found. Many of the dislocations in olivine can be seen emanating from the tips of the ilmenite inclusions. The association of dislocations and ilmenite inclusions can be thought of in one of two ways: either the inclusions nucleated first, and the dislocations were generated from the stress concentration at the tips of these inclusions, or the dislocations existed first and the inclusions precipitated preferentially on the dislocation lines. There is no definitive evidence to distinguish between these two hypotheses, however the morphology of the dislocations (Fig. 2c) seems to support the idea that the deformation event that produced the dislocation microstructure occurred after the precipitation of these inclusions. In the retrogressed peridotites, clusters of chlorite and amphibole (the products of the retrograde reactions) do not show any shape-preferred orientation. This suggests that most deformation ceased before the retrograde metamorphism occurred.

To further constrain the conditions of deformation, we relate two deformation microstructures—the olivine recrystallized grain-size and olivine LPO—to experimental data on the deformation of olivine. As we noted earlier, the clusters of similarly oriented olivine grains suggest that the olivine has completely recrystallized. From the B-type LPO, we know that this recrystallization and deformation occurred in the presence of water (>200 H/10^6 Si; Jung and Karato 2001a). Using an olivine recrystallized grain-size piezometer, we calculate that the differential stress applied during this episode of deformation was 22 ± 8 MPa (Jung and Karato 2001b). This value for stress can be inserted into a flow law for olivine (Karato and Jung 2003); given some assumptions about pressure, water content, and strain-rate, this allows us to solve for the temperature of deformation.

$$\dot{\varepsilon} = A C_{H_2O}^{r} \sigma^{n} \exp\left(-\frac{E^* + PV^*}{RT}\right) \quad (1)$$

In Eq. 1, $\dot{\varepsilon}$ is the strain-rate, A is a pre-exponential factor, C_{H_2O} is the water content, σ is the stress, r and n are constants, E^* is the activation energy, P is the

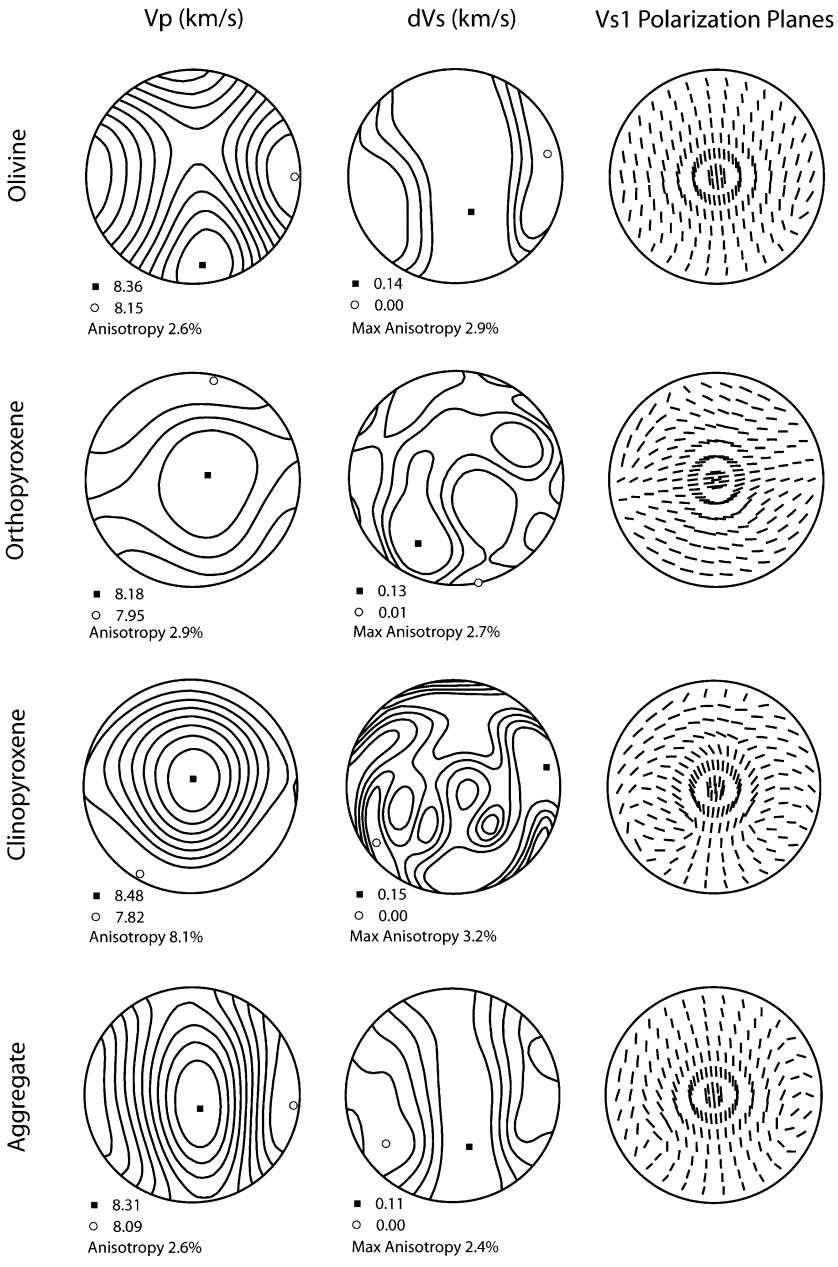

Fig. 4 Seismic anisotropy for garnet peridotite sample PK-02. These pole figures are oriented parallel to the foliation plane, with the lineation E–W. Olivine, orthopyroxene, and clinopyroxene are shown individually, and combined in normalized modal proportions (72% olivine; 17% clinopyroxene; 11% orthopyroxene). The *first column* shows P-wave azimuthal anisotropy and the *second column* shows shear-wave splitting anisotropy. The *third column* shows the polarization direction of the fast shear-wave passing through the sample in various directions. In the aggregate peridotite, fast shear-waves passing through the shear-plane will be orientated normal to the direction of shear

pressure, V^* is the activation volume, R is the gas constant, and T is the temperature. In Fig. 5, we evaluate Eq. 1 over a range of pressures at constant stress and water content. The absence of pyroxene exsolved from majorite is a strong indication that the pressure never exceeded ~6 GPa (Akaogi and Akimoto 1977). Thus, in this calculation, we consider pressures from 2 to 6 GPa. The water content during deformation is not well constrained, however it must be greater than ~200 H/10^6 Si to generate a B-type fabric (Jung and Karato 2001a) and must be less than the solubility limit of water in olivine (Kohlstedt et al. 1996). For the calculation shown in Fig. 5 we use a water content of 1,000 H/10^6 Si. For a range of reasonable geologic strain-rates (10^{-13} to 10^{-15} s^{-1}) and a range of pressures, the temperature during deformation is constrained to be 800 ± 100°C. The uncertainty in the stress measurement and the water content each contribute approximately one order of magnitude uncertainty in strain-rate. This translates into an additional uncertainty in temperature of approximately ±75°C. Thus, our conservative estimate is that the temperature during deformation was 800 ± 175°C.

This conclusion is supported by the work of Katayama and Karato (2006), who have analyzed the deformation conditions where B-type fabrics are expected to form. Using experimental data and some theoretical analysis, Katayama and Karato (2006) have shown that the B-type to C-type fabric transition is primarily dependent on temperature and stress with the B-type fabric dominating at low temperatures and/or high stresses

(Fig. 6). The temperature of the transition at reasonable geologic stresses is predicted to be between 650 and 800°C. Thus, the deformation that produced the B-type LPO at Cima di Gagnone is predicted to occur at less than 800°C, which is broadly consistent with our conclusions. Likewise, the deformation of nearby Alpe Arami, with its well-known C-type fabric (Mockel 1969; Buiskool Toxopeus 1976; Frese 2001), is predicted to occur at higher temperatures. The olivine recrystallized grain-size at Alpe Arami is not significantly different than the recrystallized grain-size at Cima di Gagnone. Thus, the stress and temperature of deformation are likely to be similar. We speculate that the deformation conditions at Cima di Gagnone and Alpe Arami narrowly bracket the B-type to C-type fabric transition temperature determined by Katayama and Karato (2006). While we do not wish to place too much emphasis on thermobarometry as it cannot be directly correlated with a specific deformation event, it is interesting to note that the equilibrium temperatures for Cima di Gagnone and Alpe Arami reported by Nimis and Trommsdorff (2001) also roughly bracket this fabric transition (740 and 830°C, respectively).

Lattice-preferred orientation and seismic anisotropy

In Frese et al. (2003) the authors studied the olivine LPO from the garnet-bearing portion of the peridotite at Cima di Gagnone. The fabrics they found had olivine [001] peaks parallel to the lineation and olivine [100] peaks normal to the foliation, and were interpreted to be C-type fabrics, similar to those documented at Alpe Arami (Mockel 1969; Buiskool Toxopeus 1976; Frese 2001). Broadly speaking, the pole figures they show are consistent with this interpretation. However, the pole figures also exhibit secondary peaks with olivine [100] axes normal to the lineation, within the foliation plane, and with olivine [010] axes normal to the foliation. These secondary peaks are consistent with a B-type fabric. Therefore, an alternative interpretation of their data would be that both the [001](100) and [001](010) slips systems contributed significantly to the development of the LPO. While we have not been able to independently confirm the presence of a C-type fabrics at Cima di Gagnone, it is reasonable to conclude that both fabrics may be present in some places, particularly since our temperature estimate places the conditions of deformation very close to the boundary between the B-type and C-type fabric regimes.

All but one sample investigated in this study show olivine B-type fabrics, which suggests that deformation occurred in the presence of at least some water (Jung and Karato 2001a; Katayama and Karato 2006). In all of the samples studied, the olivine fabric is coupled with

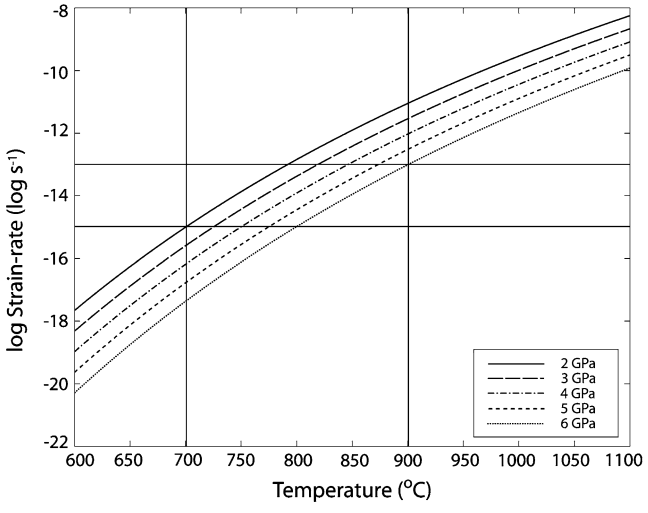

Fig. 5 Flow law for olivine deforming by dislocation creep. Curves are shown for a range of pressures (2–6 GPa) at constant stress (22 MPa) and water content (1,000 ppm H/Si). Assuming reasonable geologic strain-rates of 10^{-13} to 10^{-15} s^{-1}, the temperature of deformation is constrained to be between 700 and 900°C. Taking into account the additional uncertainty in the stress measurement and the water content, the temperature of deformation is determined to be 800 ± 175°C. The flow law is from Karato and Jung (2003); the parameters used in Eq. 1 are: $A = 10^{0.56}$ $(MPa)^{-n-r}$; $n = 3$; $r = 1.2$; $E^* = 410$ kJ/mol; $V^* = 11$ cc/mol

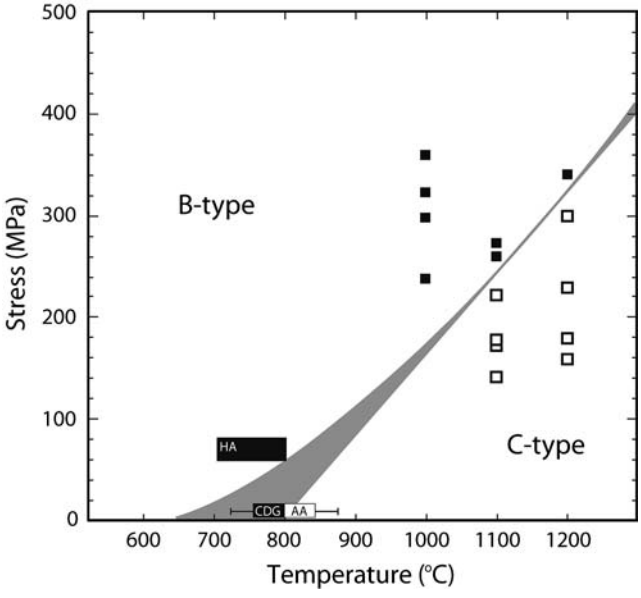

Fig. 6 B-type to C-type olivine fabric transition, modified from Katayama and Karato (2006). *Solid squares* are deformation experiments that formed B-type fabrics; *open squares* are experiments that formed C-type fabrics. Natural samples exhibiting B-type fabrics are shown as *black boxes*; natural samples exhibiting C-types fabrics are shown as *white boxes*. *HA* Higashi-akaishi (adapted from Mizukami et al. 2004), *CDG* Cima di Gagnone (this study), *AA* Alpe Arami (this study and Mockel 1969). The *gray region* indicates the location of the boundary between the B- and C-type regimes, constrained by the theory and experiments of Katayama and Karato (2006). The *error-bars* for Cima di Gagnone and Alpe Arami include the uncertainty in strain-rate, water content, and stress. The uncertainty in pressure was not included in this figure because the experimental data and data for Higashi-akaishi are all from low pressures (1–3 GPa)

a strong orthopyroxene fabric oriented in the usual way, with the [001] axes parallel to the lineation and the [100] axes normal to the foliation. Thus, we note that orthopyroxene does not display any novel fabrics at these particular deformation conditions. It is unclear whether orthopyroxene ever displays additional fabrics and experimental work covering a broad range of temperature, stress, and water content is needed. The clinopyroxene in the garnet peridotite samples also displays a strong fabric with [001] axes parallel to the lineation and [100] axes normal to the foliation. We wish to note that the small volume fraction of pyroxenes in these samples limits our ability to quantify fabric strength (Skemer et al. 2005). Nonetheless, the fabric is sufficiently strong that a qualitative assessment of fabric orientation and strength is justified.

The seismic anisotropy produced by the B-type fabric is geologically significant, because it generates shear-wave splitting with the fast shear-wave polarized normal to the direction of flow, within the shear-plane. It can therefore be used to explain the often-observed trench-parallel shear-wave splitting near subduction zones (Katayama and Karato 2006; Kneller et al. 2005). Several other studies have suggested alternative ways of generating trench-parallel seismic anisotropy, generally requiring large scale trench-parallel flow in the mantle wedge (Fischer et al. 1998; Hall et al. 2000; Peyton et al. 2001; Smith et al. 2001). While this may be reasonable under certain circumstances (e.g. Mehl et al. 2003), it requires the trench-parallel strain component to be much larger than the trench-normal strain component induced by subduction. Another model for the generation of trench-parallel shear-wave splitting has been proposed by Holtzman et al. (2003). In the Holtzman et al. (2003) model, strain in a partially molten aggregate is partitioned such that the remnant solid olivine is sheared at 90° to the macroscopic shear-direction. Thus, deformation in the A-type regime generates an apparent B-type fabric in the reference frame of the macroscopic deformation. It is this apparent B-type fabric that Holtzman et al. (2003) observe experimentally. However, if one was to examine their data in the reference frame defined by the geometry of olivine deformation, one would see an A-type fabric. In our study we investigate our samples in a reference frame defined by the shape-preferred orientation of olivine, orthopyroxene, and garnet. In other words, we observe the fabrics in the reference frame defined by the geometry of crystal deformation. Thus, the fabric we observe is an actual, not apparent, B-type fabric and cannot be explained by the Holtzman et al. (2003) model.

Conclusions

The B-type fabrics we observe at Cima di Gagnone, coupled with the well-known C-type fabrics found at Alpe Arami, provides an interesting natural laboratory for the study of the B-type to C-type fabric transition. While the metamorphic history of these rocks is still a subject of contention, we demonstrate that the deformation that produced the B-type LPO at Cima di Gagnone occurred at 800 ± 175°C. This does not preclude an earlier, higher temperature deformation event, but does indicate that the deformation that produced the B-type LPO occurred at relatively modest temperatures. Observations of the B-type fabric in the lab and in nature highlight its potential significance, and may be used to explain trench-parallel seismic anisotropy.

Acknowledgments This paper is dedicated to the late Professor Volkmar Trommsdorff, who graciously guided our visits to Cima di Gagnone and Alpe Arami. K. Kunze is thanked for his input on previous studies of Cima di Gagnone. G. Hirth and an anonymous reviewer are thanked for their help clarifying our arguments. Z. Jiang is thanked for helpful discussions, and assistance with EBSD. This study was supported by a grant from the National Science Foundation (EAR-0309448), a grant from the Geological Society of America (7526-03), and by the Japan Society for the Promotion of Sciences.

References

Abramson EH, Brown JM, Slutsky LJ, Zaug J (1997) The elastic constants of San Carlos Olivine to 17 GPa. J Geophys Res B Solid Earth Planets 102:12,253–12,263

Akaogi M, Akimoto S (1977) Pyroxene-garnet solid-solution equilibria in the systems $Mg_4Si_4O_{12}$–$Mg_3Al_2Si_3O_{12}$ and $Fe_4Si_4O_{12}$–$Fe_3Al_2Si_3O_{12}$ at high pressures and temperatures. Phys Earth Planet Inter 15:90–106

Ben Ismail W, Mainprice D (1998) An olivine fabric database; an overview of upper mantle fabrics and seismic anisotropy. Tectonophysics 296:145–157

Bozhilov KN, Green HW II, Dobrzhinetskaya L (1999) Clinoenstatite in Alpe Arami peridotite; additional evidence of very high pressure. Science 284:129–132

Buiskool Toxopeus J (1976) Peterofabrics, microtextures and dislocation substructures of olivine in a peridotite mylonite (Alpe Arami, Switzerland). Leidse Geol Meded 51:1–36

Chai M, Brown JM, Slutsky LJ (1997) The elastic constants of an aluminous orthopyroxene to 12.5 GPa. J Geophys Res B Solid Earth Planets 102:14,779–14,785

Christensen NI, Lundquist SM (1982) Pyroxene orientation within the upper mantle. Geol Soc Am Bull 93:279–288

Collins MD, Brown JM (1998) Elasticity of an upper mantle clinopyroxene. Phys Chem Miner 26:7–13

Cordellier F, Boudier F, Boullier AM (1981) Structural study of the Almklovdalen peridotite massif (southern Norway). Tectonophysics 77:257–281

Dobrzhinetskaya L, Green HW II, Wang S (1996) Alpe Arami: a peridotite massif from depths of more than 300 kilometers. Science 271:1841–1845

Durham WB, Goetze C, Blake B (1977) Plastic flow of oriented single crystals of olivine; 2, Observations and interpretations of the dislocation structures. J Geophys Res 82:5755–5770

Evans BW, Trommsdorff V (1978) Petrogenesis of garnet lherzolite, Cima di Gagnone, Lepontine Alps. Earth Planet Sci Lett 40:333–348

Fischer KM, Fouch MJ, Wiens DA, Boettcher MS (1998) Anisotropy and flow in Pacific subduction zone back-arcs. Pure Appl Geophys 151:463–475

Frese K (2001) Microstructures and lattice preferred orientation of olivine in metaperidotites (Central Alps). Doctoral Dissertation, ETH Zurich, pp 104

Frese K, Trommsdorff V, Kunze K (2003) Olivine [100] normal to foliation; lattice preferred orientation in prograde garnet peridotite formed at high H_2O activity, Cima di Gagnone (Central Alps). Contrib Mineral Petrol 145:75–86

Frisillo AL, Barsch GR (1972) Measurement of single-crystal elastic constants of bronzite as a function of pressure and temperature. J Geophys Res 77:6360–6384

Fujino K, Nakazaki H, Momoi H, Karato S-i, Kohlstedt DL (1993) TEM observation of dissociated dislocations with b = [010] in naturally deformed olivine. Phys Earth Planet Inter 78:131–137

Green HW II, Dobrzhinetskaya L, Riggs EM, Jin ZM (1997) Alpe Arami: a peridotite massif from the mantle transition zone? Tectonophysics 279:1–21

Hacker BR, et al (1997) Determining the origin of ultrahigh-pressure lherzolites: discussion and reply. Science 278:701–707

Hall CE, Fischer KM, Parmentier EM, Blackman DK (2000) The influence of plate motion on three-dimensional back arc mantle flow and shear wave splitting. J Geophys Res B Solid Earth Planets 105:28,009–28,033

Holtzman BK, et al (2003) Melt segregation and strain partitioning: implications for seismic anisotropy and mantle flow. Science 301:1227–1230

Isaak DG (1992) High-temperature elasticity of iron-bearing olivines. J Geophys Res B Solid Earth Planets 97:1871–1885

Jung H, Karato S-i (2001a) Water-induced fabric transitions in olivine. Science 293:1460–1462

Jung H, Karato S-i (2001b) Effects of water on dynamically recrystallized grain-size of olivine. J Struct Geol 23:1337–1344

Karato S-i (1987) Scanning electron microscope observation of dislocations in olivine. Phys Chem Miner 14:245–248

Karato S-i, Jung H (2003) Effects of pressure on high-temperature dislocation creep in olivine. Philos Mag 83:401–414

Katayama I, Karato S-i (2006) Wet fabric transition in olivine at low temperature: implication for flow pattern in the subduction zone. Phys Earth Planet Inter (in press)

Katayama I, Jung H, Karato S-i (2004) New type of olivine fabric from deformation experiments at modest water content and low stress. Geology 32:1045–1048

Kneller E, van Keken P, Karato S-i, Park J (2005) B-type olivine fabric in the mantle wedge: insights from high-resolution non-Newtonian subduction zone models. Earth Planet Sci Lett 237:781–797

Kohlstedt DL, Goetze C, Durham WB, Vander SJ (1976) New technique for decorating dislocations in olivine. Science 191:1045–1046

Kohlstedt DL, Keppler H, Rubie DC (1996) Solubility of water in the alpha, beta and gamma phases of $(Mg,Fe)_2SiO_4$. Contrib Mineral Petrol 123:345–357

Mainprice D (1990) A FORTRAN program to calculate seismic anisotropy from the lattice preferred orientation of minerals. Comput Geosci 16:385–393

Mehl L, Hacker BR, Hirth G, Kelemen PB (2003) Arc-parallel flow within the mantle wedge; evidence from the accreted Talkeetna Arc, south central Alaska. J Geophys Res B Solid Earth Planets 108:2375

Mizukami T, Wallis SR, Yamamoto J (2004) Natural examples of olivine lattice preferred orientation patterns with a flow-normal a-axis maximum. Nature 427:432–436

Mockel JR (1969) Structural petrology of the garnet-peridotite of Alpe Arami (Ticino, Switzerland). Leidse Geol Meded 42:61–130

Nicolas A, Christensen NI (1987) Formation of anisotropy in upper mantle peridotites: a review. In: Fuchs K, Froidevaux C (eds) Composition, structure and dynamics of the lithosphere–asthenosphere system, vol. 16. American Geophysical Union, Washington, pp 111–123

Nimis P, Trommsdorff V (2001) Revised thermobarometry of Alpe Arami and other garnet peridotites from the Central Alps. J Petrol 42:103–115

Peyton V, et al (2001) Mantle flow at a slab edge: seismic anisotropy in the Kamchatka region. Geophys Res Lett 28:379–382

Pfiffner M, Trommsdorff V (1998) The high-pressure ultramafic–mafic–carbonate suite of Cima Lunga-Adula, Central Alps: excursions to Cima di Gagnone and Alpe Arami. In: Anonymous IEC 97; 5th international eclogite conference, vol. 78. Staebli Verlag AG, Zurich, Switzerland, pp 337–354

Prior DJ, et al (1999) The application of electron backscatter diffraction and orientation contrast imaging in the SEM to textural problems in rocks. Am Mineral 84:1741–1759

Russo RM, Silver PG (1994) Trench-parallel flow beneath the Nazca Plate from seismic anisotropy. Science 263:1105–1111

Schmid SM et al (1990) The significance of the Schams Nappes for the reconstruction of the paleotectonic and orogenic evolution of the Penninic Zone along the NFP-20 East traverse (Grisons, eastern Switzerland). In: Roure F, Heitzmann P, Polino R (eds) Deep structure of the Alps, vol. 156. Societe Geologique de France, Paris, France, pp. 263–287

Skemer P, Katayama I, Jiang Z, Karato S-i (2005) The misorientation-index: development of a new method for calculating the strength of lattice-preferred orientation. Tectonophysics 411:157–167

Smith GP, et al (2001) A complex pattern of mantle flow in the Lau Backarc. Science 292:713–716

Song S, Su L (1998) Rheological properties of mantle peridotites at Yushigou in the North Qilian Mountains and their implications for plate dynamics. Acta Geol Sin (English Edition) 72:131–141

Yoshino G (1961) Structural-petrological studies of peridotite and associated rocks of the Higashiakaishi-yama District, Shikoku, Japan. J Sci Hiroshima Univ C Geol Mineral 3:343–402

Zhang S, Karato S-i (1995) Lattice preferred orientation of olivine aggregates deformed in simple shear. Nature 375:774–777